Master's Thesis
석사 학위논문

Red blood cell study at different temperatures with holographic imaging informatics

Minwoo Sim(심 민 우 沈 敏 愚)

Department of
Robotics Engineering

DGIST

2020

Master's Thesis
석사 학위논문

Red blood cell study at different temperatures with holographic imaging informatics

Minwoo Sim(심 민 우 沈 敏 愚)

Department of
Robotics Engineering

DGIST

2020

Red blood cell study at different temperatures with holographic imaging informatics

Advisor: Professor Inkyu Moon
Co-advisor: Professor Sanghyun Park

by

Minwoo Sim
Department of Robotics Engineering
DGIST

A thesis submitted to the faculty of DGIST in partial fulfillment of the requirements for the degree of Master of Science in the Department of Robotics Engineering. The study was conducted in accordance with Code of Research Ethics[1]

01. 02. 2020

Approved by

Professor Inkyu Moon (signature)
(Advisor)

Professor Sanghyun Park (signature)
(Co-Advisor)

[1] Declaration of Ethical Conduct in Research: I, as a graduate student of DGIST, hereby declare that I have not committed any acts that may damage the credibility of my research. These include, but are not limited to: falsification, thesis written by someone else, distortion of research findings or plagiarism. I affirm that my thesis contains honest conclusions based on my own careful research under the guidance of my thesis advisor.

Red blood cell study at different temperatures with holographic imaging informatics

Minwoo Sim

Accepted in partial fulfillment of the requirements for the degree of Master of Science.

11. 21. 2019

Head of Committee	Prof. Inkyu Moon	(signature)
Committee Member	Prof. Sanghyun Park	(signature)
Committee Member	Prof. Chungghiu Lee	(signature)

MS/RT
201923013

심 민 우. Minwoo Sim. Red blood cell study at different temperatures with holographic imaging informatics. Department of Robotics Engineering. 2019. 29p. Advisors Prof. Inkyu Moon, Co-Advisors Prof. Sanghyun Park

ABSTRACT

The optimal functionality of red blood cells is closely associated with the surrounding environment. This study was undertaken to analyze the changes in membrane profile, mean hemoglobin content (MCH), and cell membrane fluctuations (CMF) of healthy red blood cells (RBC) at various temperatures. The temperature was elevated from 17℃ to 41℃ within a duration of less than one hour, and the holograms were recorded by a CCD camera in an off-axis digital holographic microscopy(DHM) system. After hologram reconstruction, we extracted single RBCs and evaluated their morphologically related features (projected surface area and sphericity coefficient), MCH, and CMF. We observed that elevating the temperature results in changes in the 3D profile. Since CMF amplitude is highly correlated to the bending curvature of RBC membrane, temperature-induced shape changes can alter CMF's map and amplitude; mainly larger fluctuations appear in dimple area at a higher temperature. Regardless of the shape changes, no alterations in MCH were seen with temperature variation.

Keywords: Red blood cell, Cell membrane fluctuations, Digital holography, Homeostasis.

List of Contents

List of Figures

I. INTRODUCTION

1.1 Background

The erythrocytes and mature red blood cells (RBCs)are the main cell types in blood circulation and are also blood component. The main roles of RBCs are to carry oxygen and nutrients into the tissues and deliver carbon dioxide from the tissues to lungs to discharge out of the body. To survive for 120 days, RBCs adapt to its surroundings by ethereal adjusting of metabolism and membrane organization. Red blood cells, unlike other normal cells, lack cell organelles such as the mitochondria and nucleus or endoplasmic reticulum. This allows RBCs to increase their ability to absorb carbon dioxide and carry oxygen. The double concave shape of RBCs has the maximum surface area and flexible deformation at a given volume during the passage of microcapillaries, and these changes quickly, and the best for RBCs to survive. This is possible because RBCs do not have a three-dimensional cytoskeleton. Investigating changes in the shape of red blood cells under various conditions has long been of interest to researchers. In particular, temperature plays a universal role in steady-state volume changes, ion exchange rates, hemolysis rates, membrane dynamics, and cellular transformation[1-5]. In addition, the most important factor in blood transfusion is temperature. accordingly, research has been conducted to find a good temperature for blood transfusion. [6]. Several papers show that RBC membranes are less stable when exposed to higher temperatures than normal body temperature. One reason is that the dynamics of cell surface membranes are in turn determined by the change in the fluid state of the lipid bilayer, which is affected by temperature[7]. It is known that as the temperature increases, the membrane phospholipids of the RBCs begin to melt, eventually the RBC membranes rupture. Also, it is shown that the unilamellar state of RBC membrane is stable at the temperatures ~ 37^{o}C but at the higher temperature, it

changes to a bilayers [8]. CMF of the elastic membrane relies on the hypothesis that the driving force of fluctuations is purely thermal. Therefore, thermal changes can directly change the flickering of the membrane since it is thermally dependent. Thermally induced changes in membrane profile can also affect CMFs map and amplitude of the RBCs. It is shown that bending curvature of the RBC membrane is the main contribution of membrane fluctuations map and its magnitude [9, 10].

In this study, we monitored the changes in the shape and CMF map of RBCs by varying thetemperatures at the single-RBC level in a label-free manner. The three-dimensional (3D) images are provided by digital holography (DH) in microscopic configuration. The phase retardation can be recorded when the coherent light source travels through microscopic objects. Phase retardation is related to two factors, namely, cell thickness and the intracellular refractive index, a property linked to the water and protein content of the cells [11]. DH also provides quantitative phase images (QPI) at the single-cell level with nanometer accuracy. Since this method records phase changes instead of amplitude, staining a with a specific dyes is not required. This makes DH a well-suited technique for label-free studying. DH in microscopic configuration has been utilized in studies of various types of cells [12-20] and human red blood cells [21-27]. Parameters such as RBC volume, surface area, sphericity coefficient, refractive index and RBC membrane fluctuations are essential parameters that can be evaluated using DH.

The main motivation of this study with the previously published works is that unlike the previous work, we are very much interested in the single-RBC level changes. We are able to monitor and track the shape changes of the RBCs at the single cell level very precisely using the digital holographic microscopy. QPI image is related to two factors cell thickness and intracellular material of the RBC. Therefore, any changes in either

thickness or intracellular material for temperature changes can be monitored. We believe that we can infer an imbalance of the thermally-induced RBC membrane from changes in the parameters related to the RBCs, which can be monitored using DHM.

1.2 Label-free digital holographic imaging

The general layout of an off-axis digital holographic microscope is presented in Fig. 1(a). The hologram recording is based on the Mach-Zender interferometer. The coherent laser source is divided into object (*O*) and reference beams (*R*) by using a beam splitter (BS).

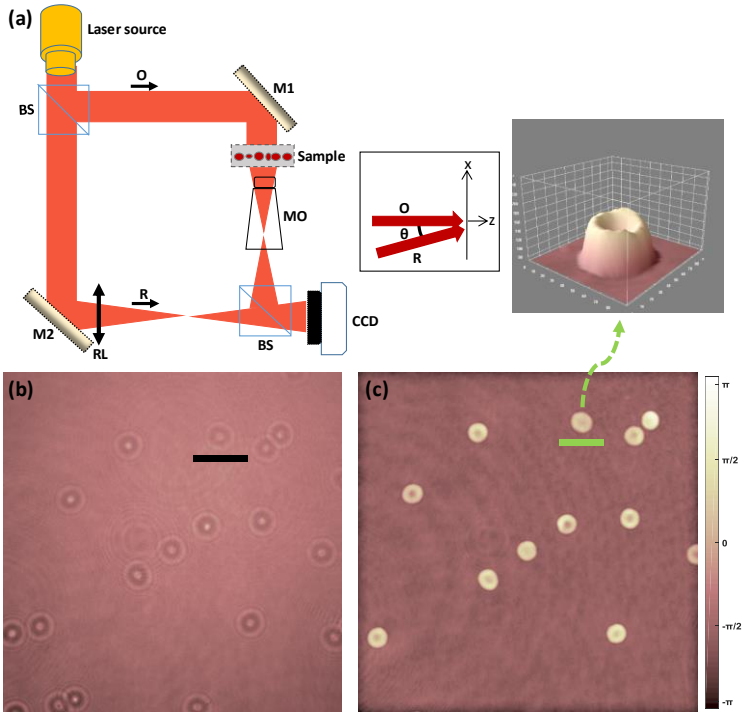

Fig. 1. Digital holographic schematic, recorded hologram and phase image.

(a) **Schematic diagram of a digital holographic in microscopic configuration; inset shows the off-axis configuration, (b) recorded hologram (black bar is 500µm), and (c) reconstructed phase image (green bar is 10µm); inset is the single cell 3D-representation**

The object beam illuminates the specimen, and a microscope objective (MO) collects and magnifies the object wave front. The object and reference wave fronts are joined by a beam splitter at a small tilt angle between them to create the off-axis hologram. At the end point, interferograms (Fig. 1(b)) are recorded by a CCD camera, and the data is transmitted to a personal computer for numerical rec onstruction.

The numerical reconstruction is explained in detail in references [28, 29]. Briefly, the interference between the object wave O and reference wave R constructs the recorded hologram I_H which is represented as:

$$I_H = |R|^2 + |O|^2 + R^*O + O^*R, \tag{1}$$

where R^* and O^* denote the complex conjugates of the reference and object beams, respectively. The small tilt angle between O and R enables us to eliminate the parasitic orders and isolate the real image from twin image and zero-order noise. In order to enable this, the digitally defined spatial filter is implemented to cover only the bandwidth of the real image. By Fourier transforming the off-axis hologram multiplying (in frequency-domain) by the filter and then applying inverse Fourier transform, only the real image information is expressed as:

$$I_H^F = IFFT\{FFT(I_H) \times Filter\} = R^*O, \tag{2}$$

where *FFT* denotes the fast Fourier transform *IFFT* denotes the inverse fast Fourier transform, and *Filter* denotes the spatial filtering in the Fourier domain. To reconstruct the phase image, the filtered hologram (I_H^F) is multiplied by the digital planer reference wave R_D:

$$R_D(k,l) = \exp\left[i\left(\frac{2\pi}{\lambda}\right)\left(k_x k\Delta x + k_y k\Delta y\right)\right], \tag{3}$$

where λ is the wavelength of the laser source, Δx and Δy are the sampling intervals in the image plane, and k_x and k_y are the wave vectors. The image reconstruction is computed by the numerical calculation of the sclar diffraction in the Fresnel approximation, which is expressed as:

$$\begin{aligned}\Psi\left(m,n\right) &= A\Phi(m,n)\exp\left[\frac{i\pi}{\lambda d}\left(m^2\Delta\xi^2 + n^2\Delta\eta^2\right)\right] \\ &\times FFT\left\{R_D\left(k,l\right)I_H^F\left(k,l\right))\times\exp\left[\frac{i\pi}{\lambda d}\left(k^2\Delta x^2 + l^2\Delta y^2\right)\right]\right\}_{m,n},\end{aligned} \tag{4}$$

where A is a complex constant value, k, l, m, and n are integers ($-N/2 \le k, l, m, n \le N/2$; and $N\times N$ is the number of pixels in the CCD camera 1024×1024). $\Phi(m,n)$ is the digital phase mask calculated by:

$$\Phi(m,n) = \exp\left[\frac{-i\pi}{\lambda D}\left(m^2\Delta\xi^2 + n^2\Delta\eta^2\right)\right], \tag{5}$$

where $\Delta\xi$ and $\Delta\eta$ are the sampling intervals in the observation plane expressed by:

$$\Delta\xi = \Delta\eta = \frac{\lambda d}{N\Delta x}, \tag{6}$$

where d denotes distance between camera plane and observation plane. A fine adjustment of k_x and k_y can be performed in the absence of fringes by removal of residual gradients or curvature of the reconstructed phase distribution in some areas of the image where a constant phase is presumed. D is the parameter that must be adjusted to compensate the wave-front curvature according to the distance between MO and specimen, and between MO and the image plane. The digital phase mask can resolve the phase aberrations caused by inserting a microscopic objective in the object wave arm, as shown in Fig. 1(a). Eventually, the phase image (Fig. 1(c)) can be obtained by the argument of:

$$\phi(x, y) = \tan^{-1}\left\{\frac{\mathrm{Im}[\Psi(m,n)]}{\mathrm{Re}[\Psi(m,n)]}\right\}, \tag{7}$$

Since the phase values are limited between $-\pi$ and $+\pi$, the result is given modulo 2π; discontinuities with values near to 2π might appear in non-flat large samples (we did not see phase jump in our RBCs). The quantitative phase image can be represented in the form of optical path differences (OPD) by:

$$OPD(x, y) = \frac{\lambda \times \phi(x, y)}{2\pi}, \tag{8}$$

OPD is related to two factors of cell thickness and the intracellular refractive index, a property linked to the protein and water content of cells. Images were acquired by off-axis DHM on a commercially available DHM T-1001 procured from LynceeTec SA (Lausanne, Switzerland) equipped with a motorized *x-y* stage (Märzhäuser Wetzlar GmbH & Co. KG, Wetzlar, Germany, ref. S429). After recording the hologram, the images were

reconstructed with a standard PC at the rate of 3 QPI images per second. For the cell membrane dynamic analysis, the sampling rate was set at 10 Hz and the sampling time was 100 seconds. We used two "MO"s of 63×/1.3NA (field of view=92μm) and 40×/0.75NA (field of view=150μm) in our configuration. The laser source (666nm) delivered an intensity of ~200μW/cm^2 to the specimen plane with an exposure time of approximately 0.4ms. Image reconstruction and all analyses were carried out using the MATLAB software.

II. METHODS

2.1 Red blood cell sample preparations

Approximately 5 ml blood was collected from three healthy male donors using a syringe. It was diluted at a ratio of 1:10 (v/v) in cold PBS buffer (pH 7.4, 138 mM NaCl, 27 mM KCl, 10mM Na2HPO4, and 1mL KH2PO4). Blood cells were sedimented by centrifuging at 200 g, 4℃ for 10 min, following which the buffy coat was gently collected, and washed once in PBS buffer for 2 min at 4 C. Finally, the isolated erythrocytes were suspended in HEPA buffer (280 mOsm, 15 mM HEPES pH 7.4, 130 mM NaCl, 5.4 mM KCl, 10 mM glucose, 1 mM CaCl2, 0.5 mM MgCl2 and 1 mg/ ml bovine serum albumin) at 0.2% hematocrit; 1 ml of the erythrocyte suspension was diluted to 15 ml using HEPA buffer. Two experimental conditions were considered. For the first experiment, ~40 μl of the final erythrocyte suspension was introduced into the imaging slide consisting of two coverslips. The bottom coverslip was coated with polyornithine to ensure that cells adhere to the coverslip surface. For the second experiment, 200 μl of the final erythrocyte suspension was dropped on

the 18mm imaging slide of a round chamber. The glass and chamber were mounted on the DHM device and incubated for 10 minutes at 17℃ under conditions of 5% CO2 and high humidity (Chamlide WP incubator system, LCI, Seoul, South Korea). This ensures that the cells adhere well to the glass. For the RBC membrane fluctuation analysis, the RBCs were imaged at 17℃, 23℃, 37℃ and 41℃, with the sensitivity of ±0.1℃. The RBCs were imaged continually for all other parameters. Only cells with the discocyte morphology (n>=36) are considered for the final analysis; all other morphologies are excluded from the sample set.

All the blood samples in this study were obtained with informed consent from all subjects. All procedures were performed in accordance with the internal protocols of our laboratory, which is in accordance with the guide-lines and regulations (DGIST-180713-BR-012-01) approved by the bio-safety committee, DGIST University, Korea and institutional review boards (IRBs) in Korea. The experiments were finished within a few hours after sample collection.

III. RESULTS AND DISCUSSIONS

3.1 Biochemical and morphological parameters

Several parameters related to the morphological aspects, RBC membrane fluctuations and clinically relevant at the single-RBC level, were analyzed. Before analysis, several single RBCs (only RBCs with the perfect biconcave morphology) were manually extracted from the original QPI images (see Fig. 1(c) and the inset). Single cells were then binarized to provide background and cell region masks. The morphological operation of dilation was applied to the background mask to isolate it from the sell area. The first morphologically relevant variable was the projected surface area (PSA), defined as:

$$PSA = Np^2, \tag{9}$$

where N is the total number of pixels within the RBC projected area resulting from the image binarization. MCH is a clinically relevant parameter that can be evaluated by interferometric methods such as DHM. Phase retardation is proportional to the protein component of the cell and, in case of RBCs, is mostly composed of hemoglobin. The refractive index is closely related to other properties of the red cell (volume, size, water content, temperature changes) and depends considerably on the cell environment. The individual dry weight of a red cell, however, is a property which remains more or less unchanged when it has reached a final value during the maturation process of the reticulocyte:

$$MCH = \frac{10 \times \overline{OPD} \times (PSA)}{\lambda \alpha_{HB}}, \tag{10}$$

where $\overline{OPD}$ is the average optical path difference (OPD) over the projected surface area of the cell (see Eq. 11), λ is the wavelength of the light source of the setup, and α_{HB} =0.00196 *dl*/*g* is the specific refraction increment related mainly to the protein concentration of hemoglobin.

$$\overline{OPD} = \sum_{(i,j)\in S_p} OPD(i, j), \tag{11}$$

where the summation achieved considering all the pixels (i,j) belongs to the projected surface S_p of the RBC, and $OPD(i, j)$ is the OPD value at pixel (i, j). Another morphological property is the sphericity coefficient k, which is expressed as the ratio of the OPD value, OPD_c, at the RBC center to the OPD value at half of its radius (OPD_t):

$$k = \frac{OPD_c}{OPD_r}, \tag{12}$$

RBC membrane fluctuations were also measured during the period of temperature changes. For this analy-

sis, four temperatures were considered: 17°C, 23°C, 37°C and 41°C. At each temperature, we recorded 100 holograms having sampling rate of 10Hz. Holograms were numerically reconstructed after the experiment. The model for measuring the RBC membrane fluctuations is presented in the following references [23, 24].

Briefly, a region of interest (ROI) with two independent variables are required;

$std(OPD_{cell} + OPD_{bkgd})(x, y)$ which is the temporal deviation within the RBC area (combining both the cell fluctuations and noise), and $std(OPD_{bkgd})$ which is the mean of the temporal deviation of all the pixels outside the RBC area. Accordingly, the fluctuations for each single pixel *CMF(x,y)* is evaluated by the formula:

$$CMF_{RBC}(x, y) = \sqrt{\left(std\left(OPD_{cell} + OPD_{bkgd}\right)(x, y)\right)^2 - \left(std\left(OPD_{bkgd}\right)\right)^2}, \tag{13}$$

3.2 Discussions

3.2.1 RBC trapped between cover slip and glass

Fig. 2 shows RBC images at different temperature and the profile and cross-section of one RBC at two temperatures, 17°C and 41°C. This is the case when cells are trapped between cover slip and glass. As is clearly observed, the dimple section (central portion) of the RBC differs at both temperature parameters.

The impact of increasing temperature was assessed by measuring the morphological parameters, MCH and magnitude of fluctuation rates. Fig. 3(a) shows the change of temperature with time, wherein we observe that MCH remains unchanged (Fig. 3(b)), and showing only minor fluctuations around its average value (30.76pg). As the temperature increases, the PSA increases and the spherical coefficient decreases. (see Fig. 3(c) & (d)). The results suggest that RBCs lose the intracellular fluid and consequently the volume of RBC drops. At the beginning of the experiment, the cells and extracellular medium are in an isotonic state, so no

movement of water has occurred, and the RBCs can preserve their shape.

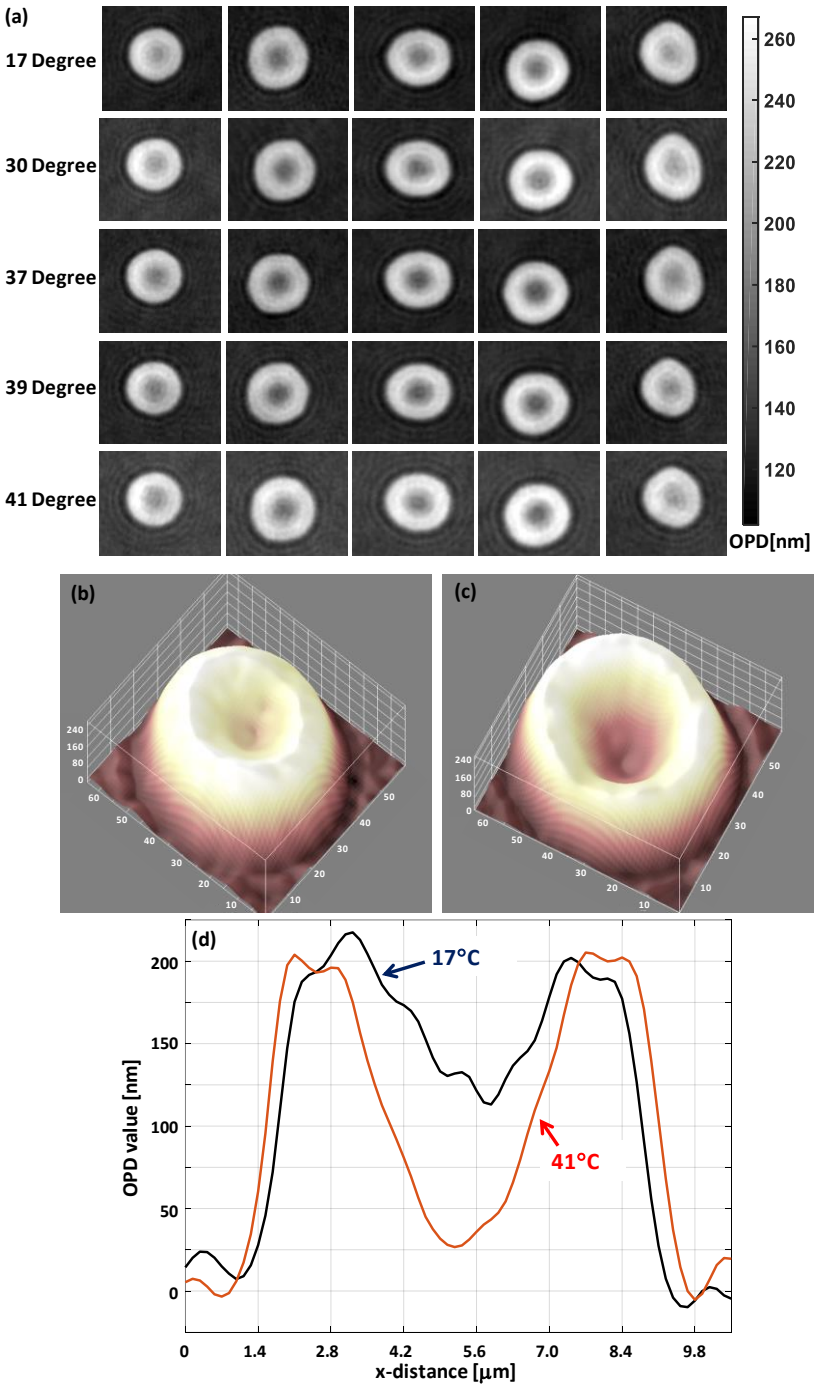

Fig. 2. Shape change of RBC trapped between cover slip and glass at different temperatures.

(a) Gallery of RBC images; same RBCs are shown at different temperatures, (b) RBC at 17°C, (c) the same RBC at 41°C, and (d) cross-section of (b) and (c) drawn together. PSA for the RBC in (b) and (c), respectively, are 60µm^2 and 64µm^2. Sphericity coefficient for the RBC in (b) and (c), respectively, are 0.65 and 0.45. MCH=32.3pg and 32.5pg for RBC shown in (b) and (c), respectively.

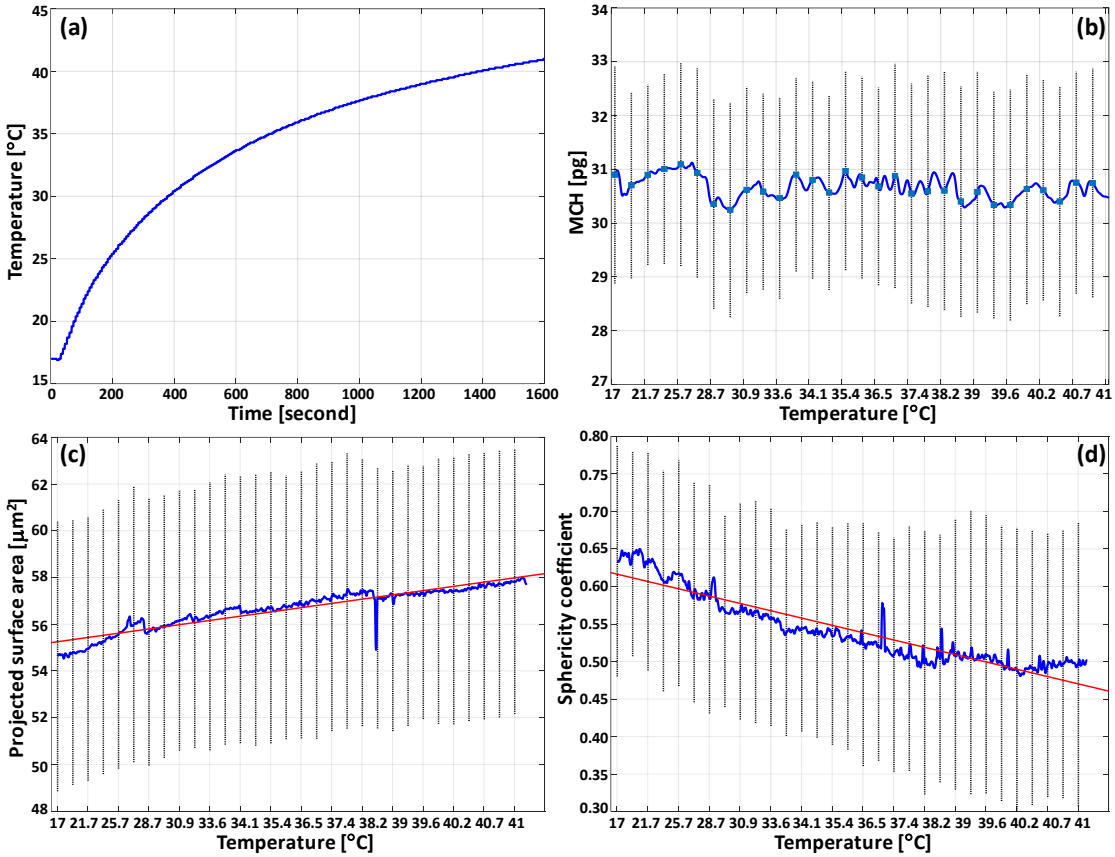

Fig. 3. Result of parameters related to RBCs trapped between cover slip and glass.

(a) Temprature change of the sample with time, (b) MCH, (c) projected surface area, and (d) sphericity coefficient changes versus temperature elevation (n >= 36 cells). F-statistics performed on data shown in (c) and (d) suggests that the slope of the linear regression line is significantly different from zero; p-value < 0.05. Error bars shown in the plots represent twice the corresponding standard deviations.

After some moments of increasing temperature, the surrounding medium gradually starts to evaporate, causing an imbalance between the intracellular and extracellular fluids. It also increases intracellular fluidity since it is directly affected by the higher temperature. Therefore, a concentration gradient is created between the RBC membrane and the extracellular medium is created, and water molecules begin to leave the RBC to reduce the gradient. This causes the RBC to lose water resulting in a decrease in volume. Also, this causes an

increase in the concentration of the material inside the RBC compared to the conditions at low temperatures. This is due to the lack of water inside the RBC at higher temperatures. We cannot fully confirm the volume loss because the refractive index of RBC is required to convert OPD value to actual RBC thickenss and then calculate the volume. The RBC's refractive index is obtained at the room temperature, but it depends on the temperature. Additionally, if there is a change in concentrations of materials within the RBC, it changes integral refractive index of RBC.

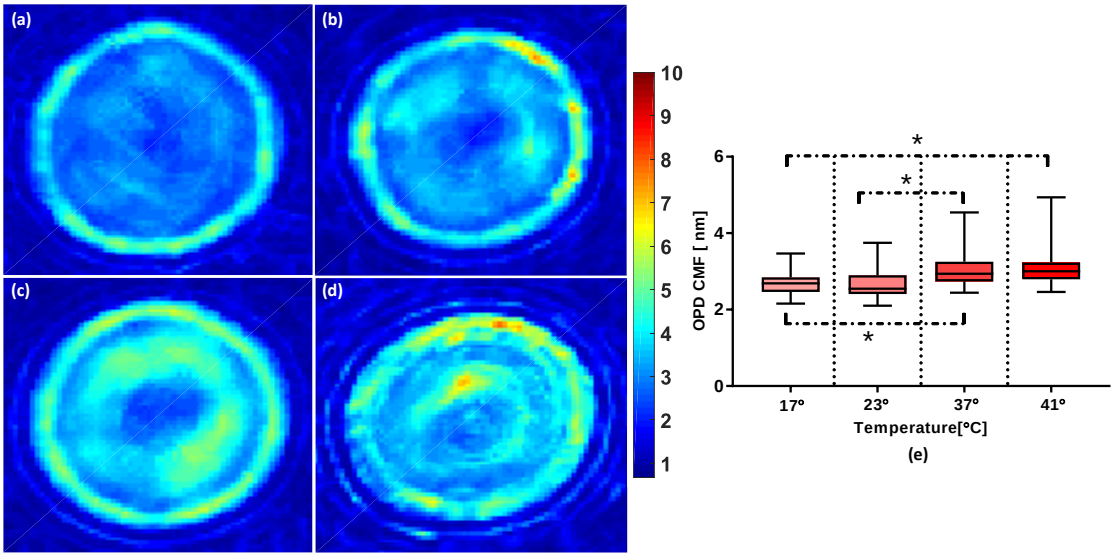

Fig. 4. Fluctuations map for an RBC trapped between cover slip and glass at different temperatures.

Fluctuations map for an RBC at different temperatures. (a) 17°C, (b) 23°C, (c) 37°C, (d) º41°C, (e) box plot representation of amplitude of CMF for the four different temperatures. An asterisk * indicates that results are significantly different according to the two-sample Kolmogorov-Smirnov test; p-value < 0.05.

Fig. 4 show the CMF maps for RBC measured at four different temperatures. The deviations map of the cell is evaluated by Eq. (13). We calculate the $std(OPD_{cell}+OPD_{bkgd})(x,y)$, which is the temporal deviation within the ROI that combines both the cell fluctuations and noise. Furthermore, we also calculate the average

value of $std(OPD_{bkgd})$, which is the temporal deviation of all the pixels outside the projected area of the RBC. The two measured values are substituted into Eq. (13) to evaluated the map. The CMF amplitude of the entire cell is the average of the CMF(x,y) over the projected area of the entire cell. The CMF amplitude for each temperature is also calculated, and the comparison is shown by a box plot (Fig. 4(e)). It is clearly observed in Fig. 4 that the CMF map at lower temperatures predominates at the ring section of the membrane. Popescu showed that RBC membrane fluctuations is directly related to the Gaussian curvature of RBC [9]. The deformation of membrane is dominant at the area in which the Gaussian curvature approaches zero. At higher temperatures, intracellular fluids are lost, which in turn resulted in an RBC with smaller sphericity coefficient. Thus, the Gaussian curvature is modified and then, fluctuations map is different at higher temperatures. We also found a significant negative correlation between CMF values and sphericity coefficients in previous work [25]. In addition, the Kolmogorov-Smirnov test shows that the CMF of the ring is greater than the corresponding value in the dimple section for all temperatures (data not shown here).

It is worth mentioning that no changes in morphology, shape, and CMF are observed when the cells are left at room temperature for one hour (data not shown here).

3.2.1 RBCs imaged on chamber:

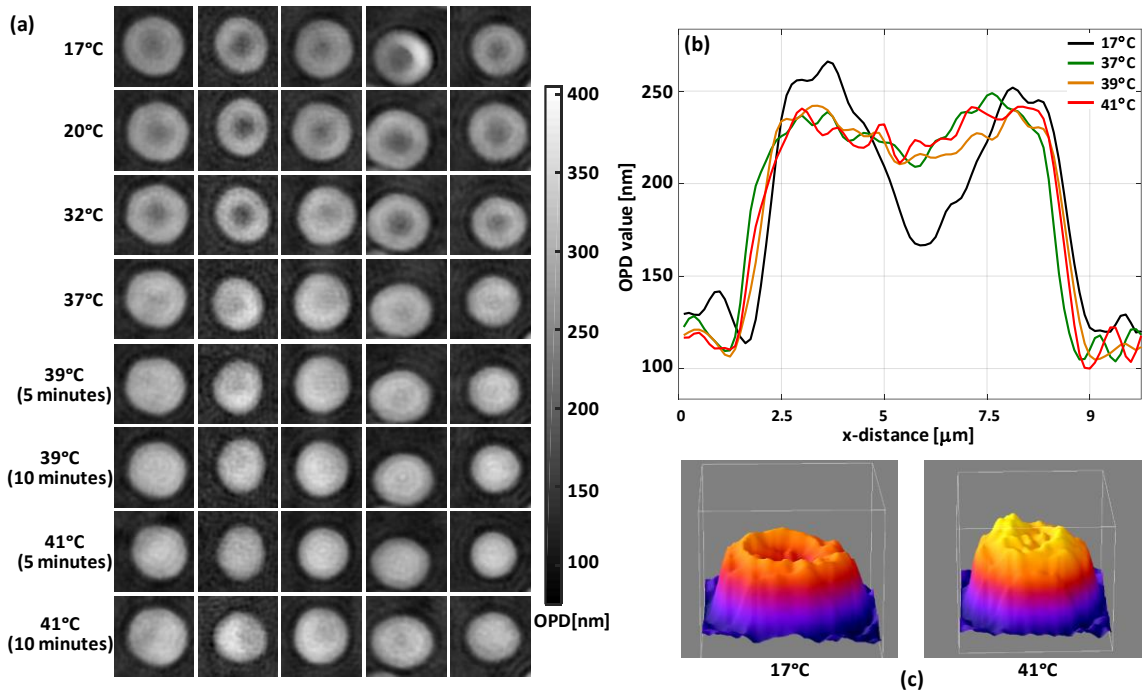

Fig. 5. Shape change results in chamber at different temperature.

(a) Gallery of RBC images; same RBCs are shown at different temperatures, (b) cross-section of the same RBC shown at different temperature (c) 3D representation of the RBC in 17ºC and 41ºC. PSA for the RBC in (b) and (c), respectively, are 49µm2 and 50µm2. Sphericity coefficient for the RBC in (b) and (c), respectively, are 0.86 and 0.91. MCH=30.5pg and 30.9pg for RBC shown in (b) and (c), respectively.

In the second experiment 200µl of the suspension was dropped onto the imaging glass of an 18mm round coverslip chamber. The temperature was elevated and RBCs were imaged. RBCs were imaged at each temperature. 5 and 10 minutes after that temperature reached the desired level. Fig. 5 shows a gallery of RBC images at different temperatures and the profile of one RBC at different temperature.

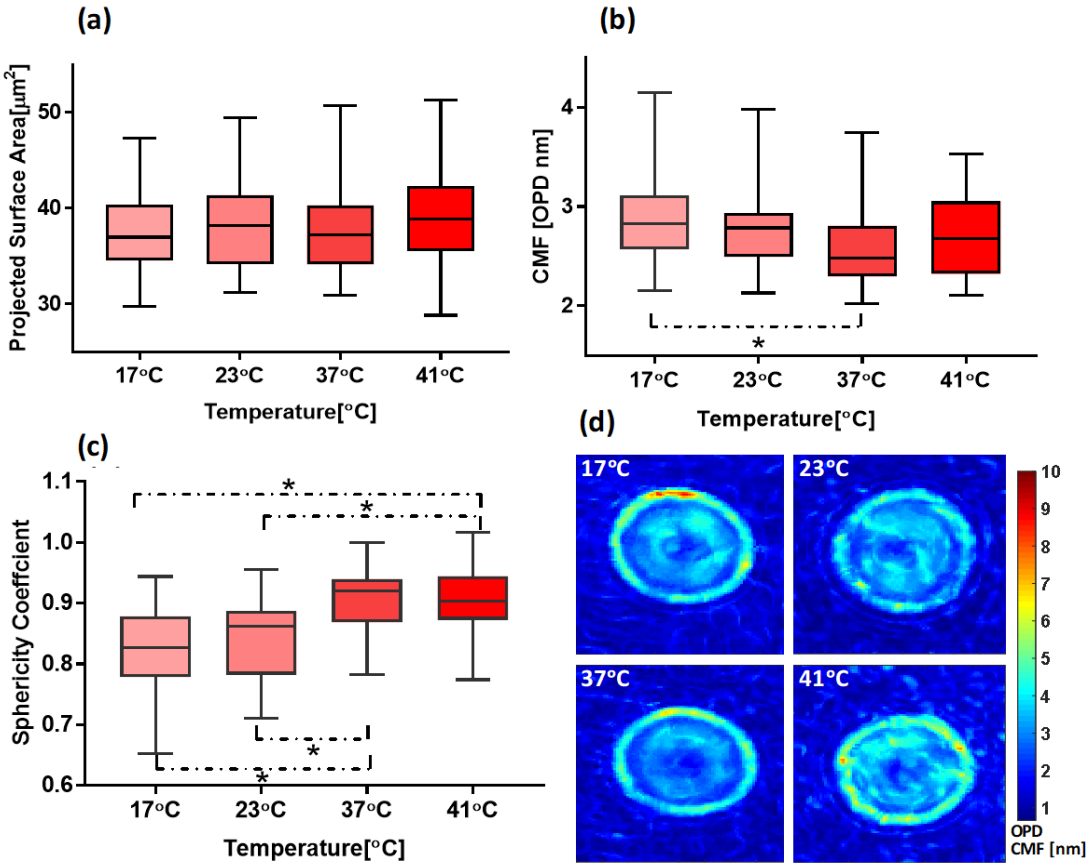

Fig. 6. Result of parameters related to RBCs in chamber.

(a) Projected surface area, (b) CMF value and (c) sphericity coefficient at different temperatures (d) represents CMF map at different temperatures. An asterisk * indicates that results are significantly different according to the two-sample Kolmogorov-Smirnov test; p-value < 0.05; n >= 36 cells).

Fig. 6 shows the effect of temperature elevation on the shape and membrane fluctuations. It can be readily seen that the sphericity coefficient of the RBC at a lower temperature is less than the same value at a higher temperature. No significant change in PSA is observed but CMF value for two temperature of 17ºC and 37ºC are significantly different ($p<0.005$). The mean corpuscular volume of the samples was measured with a Sysmex XP-300 Impendence Volume Analyzer, which is commonly used to obtain total blood counts in hematology laboratories. No changes in volume or MCH are found at different temperatures (data not shown here). We did not observe significant reversible changes in the membrane of the RBCs and the cells preserved their

shape. It is worth mentioning that some RBCs are gradually starting to lose their membrane stability. Accordingly, RBCs with spiculated shape started to appear.

The cell membrane is made up of phospholipids which are rather fluid. The phospholipids are more rigid at lower temperatures and it becomes soften at the higher temperatures. More specifically, the fatty acid tails of the phospholipids become less rigid, allowing more movement of proteins and other molecules within and through the membrane. At some temperatures above normal ambient level, the membrane is more unstable and very fluid. Another hypothesis is that the transformation of the membrane bilayer occurs when the normal ambient temperature of the cell is exceeded. Accordingly, the growth temperature of the cell is a critical point at which optimal membrane bilayer stability occurs.

IV. CONCLUSIONS

The mechanical properties and shape of cells can be modified by temperature changes. In this paper, we analyzed the effect of temperature on several parameters of RBCs by using digital holographic microscopy. The temperature was elevated for less than one hour. Our results indicate that although there are changes in some parameters related to the profile of RBC, RBCs retain their normal morphology. The sphericity coefficient changes when The temperature of the cell changes. Another hypothesis is that temperature enhances the fluidity of some membrane compounds.

Abbreviations

MCH: mean hemoglobin content

CMF: cell membrane fluctuations

RBC: red blood cell

ATP: Adenosine Triphosphate

3D: Three-dimensional

QPI: quantitative phase image

DH: digital holography

DHM: digital holographic microscopy

MO: microscope objective

CCD: charge coupled device

OPD: optical path differences

PSA: projected surface area.

References

[1] Ben-Isaac, Eyal, et al. “Effective temperature of red-blood-cell membrane fluctuations,” Physical review letters 106.23 (2011): 238103.

[2] Evans, James, et al. “Fluctuations of the red blood cell membrane: relation to mechanical properties and lack of ATP dependence,” Biophysical journal 94.10 (2008): 4134-4144.

[3] Choi, Wonjune, Juyeon Yi, and Yong Woon Kim. “Fluctuations of red blood cell membranes: The role of the cytoskeleton,” Physical Review E 92.1 (2015): 012717.

[4] Boss, Daniel, et al. “Spatially-resolved eigenmode decomposition of red blood cells membrane fluctuations questions the role of ATP in flickering,” PLoS One 7.8 (2012): e40667.

[5] Waugh, R., and E. A. Evans. “Thermoelasticity of red blood cell membrane,” Biophysical journal 26.1 (1979): 115-131.

[6] Uhl, Lynne, Donna Pacini, and Margot S. Kruskall. “A comparative study of blood warmer performance,” Anesthesiology 77.5 (1992): 1022-1028.

[7] Gottlieb, Melvin H., and E. D. Eanes. “On phase transitions in erythrocyte membranes and extracted membrane lipids,” Biochimica et Biophysica Acta (BBA)-Biomembranes 373.3 (1974): 519-522.

[8] Gershfeld, Norman L., and Makio Murayama. “Thermal instability of red blood cell membrane bilayers: temperature dependence of hemolysis,” The Journal of membrane biology 101.1 (1988): 67-72.

[9] Popescu, Gabriel, et al. “Optical measurement of cell membrane tension,” Physical review letters 97.21 (2006): 218101.

[10] Evans, Arthur A., et al. “Geometric localization of thermal fluctuations in red blood cells,” Proceedings of the National Academy of Sciences 114.11 (2017): 2865-2870.

[11] Barer, R. “Interference microscopy and mass determination,” Nature 169.4296 (1952): 366-

367.

[12] Moon, Inkyu, et al. “Automated three-dimensional identification and tracking of micro/nanobiological organisms by computational holographic microscopy,” Proceedings of the IEEE 97.6 (2009): 990-1010.

[13] Javidi, Bahram, et al. “Three-dimensional imaging and recognition of microorganism using single-exposure on-line (SEOL) digital holography,” Optics Express 13.12 (2005): 4492-4506..

[14] Moon, Inkyu, and Bahram Javidi. “3-D visualization and identification of biological microorganisms using partially temporal incoherent light in-line computational holographic imaging,” IEEE transactions on medical imaging 27.12 (2008): 1782-1790.

[15] Rappaz, Benjamin, et al. “Measurement of the integral refractive index and dynamic cell morphometry of living cells with digital holographic microscopy,” Optics express 13.23 (2005): 9361-9373.

[16] Dubois, Frank, et al. “Digital holographic microscopy for the three-dimensional dynamic analysis of in vitro cancer cell migration,” Journal of biomedical optics 11.5 (2006): 054032.

[17] Anand, Arun, Inkyu Moon, and Bahram Javidi. “Automated disease identification with 3-D optical imaging: a medical diagnostic tool,” Proceedings of the IEEE 105.5 (2017): 924-946.

[18] Merola, F., et al. “Digital holography as a method for 3D imaging and estimating the biovolume of motile cells,” Lab on a Chip 13.23 (2013): 4512-4516.

[19] Rappaz, Benjamin, et al. “Automated multi-parameter measurement of cardiomyocytes dynamics with digital holographic microscopy,” Optics express 23.10 (2015): 13333-13347.

[20] Rappaz, Benjamin, et al. “Noninvasive characterization of the fission yeast cell cycle by monitoring dry mass with digital holographic microscopy,” Journal of biomedical optics 14.3 (2009): 034049.

[21] Moon, I., et al. “Identification of Malaria-infected red blood cells via digital shearing interferometry and statistical inference,” IEEE Photonics Journal 5.5 (2013): 6900207-6900207.

[22] Rappaz, Benjamin, et al. “Comparative study of human erythrocytes by digital holographic microscopy, confocal microscopy, and impedance volume analyzer,” Cytometry Part A: the journal of the International Society for Analytical Cytology 73.10 (2008): 895-903.

[23] Jaferzadeh, Keyvan, and Inkyu Moon. “Human red blood cell recognition enhancement with three-dimensional morphological features obtained by digital holographic imaging,” Journal of biomedical optics 21.12 (2016): 126015.

[24] Rappaz, Benjamin, et al. “Spatial analysis of erythrocyte membrane fluctuations by digital holographic microscopy,” Blood Cells, Molecules, and Diseases 42.3 (2009): 228-232.

[25] Jaferzadeh, Keyvan, et al. “Quantification of stored red blood cell fluctuations by time-lapse holographic cell imaging,” Biomedical optics express 9.10 (2018): 4714-4729.

[26] Moon, Inkyu, et al. “Automated quantitative analysis of 3D morphology and mean corpuscular hemoglobin in human red blood cells stored in different periods,” Optics express 21.25 (2013): 30947-30957.

[27] Javidi, Bahram, et al. “Sickle cell disease diagnosis based on spatio-temporal cell dynamics analysis using 3D printed shearing digital holographic microscopy,” Optics express 26.10 (2018): 13614-13627.

[28] Colomb, Tristan, et al. “Numerical parametric lens for shifting, magnification, and complete aberration compensation in digital holographic microscopy,” JOSA A 23.12 (2006): 3177-3190.

[29] Colomb, Tristan, et al. “Automatic procedure for aberration compensation in digital holographic microscopy and applications to specimen shape compensation,” Applied optics 45.5 (2006): 851-863.

요 약 문

디지털 홀로그래피를 이용한 온도변화에 따른 적혈구 3 차원 형상 및 운동성 특성 조사

본 논문에서는 적혈구의 기능이 주변환경과 밀접한 관계에 있는데, 디지털 홀로그래피와 영상처리 결합 기술 기반으로 온도변화에 따른 건강한 적혈구의 표면적, 평균 위상 값, 질량, 세포막 변동률 등과 같은 여러 중요 임상 파라미터 값들에 대한 특성 값을 정량적으로 분석하는 방법론을 제안하였으며, 흥미롭게도, 온도변화에 따른 적혈구세포의 형태학적인 특성 및 세포막 변동률 값 측정을 기반으로 적혈구세포의 구형 계수와 온도 간에 유의미한 상관 관계가 있음을 발견했다. 또한 온도가 높은 적혈구의 세포막 변동률 값이 온도가 낮은 경우보다 상대적으로 커짐을 발견하였으며, 그리고 온도 변화에 따라 모양 변화에 관계없이 적혈구세포의 질량의 변화는 나타나지 않음을 실험결과를 통하여 입증하였다.

핵심어: : 적혈구세포 형상분석, 세포막 변동률 분석, 디지털 홀로그래픽 현미경, 항상성